Received: 7 March 2024 | Revised: 11 April 2024 | Accepted: 14 April 2024

DOI: 10.1002/agt2.571

Aggregate WILEY

RESEARCH ARTICLE

Highly efficient organic light-emitting diodes and light-emitting electrochemical cells employing multiresonant thermally activated delayed fluorescent emitters with bulky donor or acceptor peripheral groups

Jingxiang Wang[1] | **Hassan Hafeez**[2] | **Shi Tang**[3] | **Tomas Matulaitis**[1] | **Ludvig Edman**[3] | **Ifor D. W. Samuel**[2] | **Eli Zysman-Colman**[1]

[1]Organic Semiconductor Centre, EaStCHEM School of Chemistry, University of St Andrews, St Andrews, Fife, UK

[2]Organic Semiconductor Centre, SUPA School of Physics and Astronomy, University of St Andrews, St Andrews, UK

[3]The Organic Photonics and Electronics Group, Department of Physics, Umeå University, Umeå, Sweden

Correspondence
Eli Zysman-Colman, Organic Semiconductor Centre, EaStCHEM School of Chemistry, University of St Andrews, St Andrews, Fife, KY16 9ST, UK.
Email: eli.zysman-colman@st-andrews.ac.uk

Ifor D. W. Samuel, Organic Semiconductor Centre, SUPA School of Physics and Astronomy, University of St Andrews, St Andrews, KY16 9SS, UK.
Email: idws@st-andrews.ac.uk

Ludvig Edman, The Organic Photonics and Electronics Group, Department of Physics, Umeå University, SE-90187, Umeå, Sweden.
Email: ludvig.edman@umu.se

Funding information
Engineering and Physical Sciences Research Council, Grant/Award Numbers: EP/R035164/1, EP/W007517/1, EP/W015137/1; China Scholarship Council, Grant/Award Number: 202006250026; Swedish Energy Agency, Grant/Award Numbers: 50779-1, P2021-00032; Swedish Research Council, Grant/Award Numbers: 2019-02345, 2021-04778; European Research Council, Grant/Award Number: 101096650; Knut och Alice Wallenbergs Stiftelse, Grant/Award Number: WISE-AP01-D02

Abstract

Multiresonant thermally activated delayed fluorescence (MR-TADF) emitters have been the focus of extensive design efforts as they are recognized to show bright, narrowband emission, which makes them very appealing for display applications. However, the planar geometry and relatively large singlet–triplet energy gap lead to, respectively, severe aggregation-caused quenching (ACQ) and slow reverse intersystem crossing (RISC). Here, a design strategy is proposed to address both issues. Two MR-TADF emitters triphenylphosphine oxide **(TPPO)-tBu-DiKTa** and triphenylamine **(TPA)-tBu-DiKTa** have been synthesized. Twisted *ortho*-substituted groups help increase the intermolecular distance and largely suppress the ACQ. In addition, the contributions from intermolecular charge transfer states in the case of **TPA-tBu-DiKTa** help to accelerate RISC. The organic light-emitting diodes (OLEDs) with **TPPO-tBu-DiKTa** and **TPA-tBu-DiKTa** exhibit high maximum external quantum efficiencies (EQE_{max}) of 24.4% and 31.0%, respectively. Notably, the device with 25 wt% **TPA-tBu-DiKTa** showed both high EQE_{max} of 28.0% and reduced efficiency roll-off (19.9% EQE at 1000 cd m^{-2}) compared to the device with 5 wt% emitter (31.0% EQE_{max} and 11.0% EQE at 1000 cd m^{-2}). The new emitters were also introduced into single-layer light-emitting electrochemical cells (LECs), equipped with air-stable electrodes. The LEC containing **TPA-tBu-DiKTa** dispersed at 0.5 wt% in a matrix comprising a mobility-balanced blend-host and an ionic liquid electrolyte delivered blue luminance with an EQE_{max} of 2.6% at 425 cd m^{-2}. The high efficiencies of the OLEDs and LECs with **TPA-tBu-DiKTa** illustrate the potential for improving device performance when the DiKTa core is decorated with twisted bulky donors.

KEYWORDS
aggregation-caused quenching, electroluminescence, long-range charge transfer, OLED, organic semiconductor, short-range charge transfer, TADF

1 | INTRODUCTION

Thermally activated delayed fluorescence (TADF) emitters have been widely investigated in organic light-emitting diodes (OLEDs)[1–3] and to a lesser extent in light-emitting electrochemical cells (LECs).[4–6] A conventional TADF molecule contains electron donor (D) and acceptor (A) groups that are weakly electronically conjugated. This is due to the presence of a large dihedral angle between the two that results in a weak overlap between the highest

Jingxiang Wang, Hassan Hafeez, and Shi Tang contributed equally to this work.

occupied molecular orbital (HOMO) and the lowest unoccupied molecular orbital (LUMO). The resulting small singlet–triplet energy gap (ΔE_{ST}) provides an avenue to harvest 100% of the electrically generated excitons in the device through reverse intersystem crossing (RISC) prior to emission from the S_1 state.[7] However, due to the large degree of structural relaxation in the S_1 state as a result of its long-range charge transfer (LRCT) character, the emission of D–A type compounds is broad, leading to poor color saturation.[8]

In 2016, Hatakeyama et al. reported a new class of TADF compounds, known as multiresonant TADF (MR-TADF) emitters.[9] In these compounds, electron-donating and electron-accepting atoms are embedded within a polycyclic aromatic framework. The complementary mesomeric effects of these atoms produce an alternating pattern of increasing and decreasing electron density in the excited states compared to the ground state, resulting in a modest ΔE_{ST}. The short-range charge transfer (SRCT) character of the emissive S_1 state and the rigid structure results in small Stokes shifts, narrowband emission, and high photoluminescence (PL) quantum yields (Φ_{PL}). MR-TADF emitters can basically be divided into two categories based on the nature of the acceptor: boron-based emitters and carbonyl-based emitters. The first carbonyl-based MR-TADF emitter (**DiKTa**, aka **QAO**, **QAD**) was reported by both us[10] and Jiang, Liao, and coworkers.[11,12] It emits at λ_{PL} of 466 nm with a full width at half maximum (FWHM) of 32 nm and has a ΔE_{ST} of 0.18 eV in toluene. As 5 wt% doped film in 1,3-bis(*N*-carbazolyl) benzene (mCP), this compound has a Φ_{PL} of 72.4% and a delayed lifetime τ_d of 93 µs. Depending on the device configuration, the OLEDs showed a maximum external quantum efficiency (EQE_{max}) of 19.4% at the electroluminescence (EL) peak wavelength (λ_{EL}) of 468 nm[11] or an EQE_{max} of 14.7% at λ_{EL} of 465 nm.[10]

Since these initial reports, many **DiKTa**-based MR-TADF emitters have been reported.[12–27] The structures and properties are summarized in the Electronic Supporting Information (ESI) (Figures S23–S25 and Table S10). Of particular relevance, Chen et al. reported a derivative of DiKTa, **MTDMQAO**, containing a 2,4-dimethyl-1,3,5-triazine acceptor.[26] **MTDMQAO** exhibits narrowband blue emission at λ_{PL} of 455 nm (FWHM of 19 nm) and has a ΔE_{ST} of 0.20 eV in toluene. The Φ_{PL} is near unity at 99% and the τ_d is 32 µs in the 10 wt% doped film in mCP. The OLEDs with **MTDMQAO** showed high EQE_{max} of 29.4% at λ_{EL} of 472 nm. We reported the emitter **3TPA-DiKTa**, which contains three triphenylamine (TPA) donors about the central **DiKTa** core.[20] In 2 wt% doped films in mCP, **3TPA-DiKTa** emits at λ_{PL} of 551 nm (FWHM of 58 nm), has a ΔE_{ST} of 0.13 eV and a τ_d of 131 µs. The devices achieved very high EQE_{max} of 30.8% at 552 nm (FWHM of 62 nm).

In addition, when connected to strong donors, **DiKTa** can also act as an acceptor in D–A TADF emitters. Yuan et al. first reported **QAO-DAd** with two 9,9-dimethyl-9,10-dihydroacridine (DMAC) as donors.[11] **QAO-DAd** emits at λ_{PL} of 548 nm in toluene, has a high Φ_{PL} of 89.8% and a small ΔE_{ST} of 0.01 eV in 5 wt% doped films in 4,4'-di(9*H*-carbazol-9-yl)-1,1'-biphenyl (CBP). The OLED showed an EQE_{max} of 23.9% at λ_{EL} of 552 nm. Our group reported a series of **DiKTa**-based D–A TADF emitters using donors with different electron-donating abilities.[16] **DMAC-DiKTa**, with a Φ_{PL} of 76% and a ΔE_{ST} of 0.04 eV, produced the highest device performance, with an EQE_{max} of 23.8% at λ_{EL} of 549 nm and with a low efficiency roll-off of 16.4% at 1000 cd m^{-2}.

Although OLEDs employing **DiKTa**-based TADF emitters have achieved excellent EQE_{max}, aggregation remains an issue at higher doping concentrations within the emissive layer,[28,29] resulting in aggregation-caused quenching (ACQ) and undesired exciton annihilation processes.[30] Low emitter doping concentrations are usually required within the emitting layers (EML) to alleviate this problem. However, a very low doping of the emitter in the host leads to a narrower exciton recombination zone within the emitting layer. The high concentration of excitons formed in host materials at high voltage is more likely to undergo bimolecular quenching processes such as triplet–triplet or triplet–polaron annihilation, which results in severe efficiency roll-off at high current density and poor device stability.[31] In addition, there have been only a few reports of MR-TADF LECs[4,22,32,33] (Figure S25 and Table S11) and their efficiencies are much worse than those of D–A TADF LECs.[5] Thus, there remains outstanding materials and device efforts to demonstrate the potential of MR-TADF LECs to deliver color-saturated high efficiency devices.

Here, we report two new **DiKTa**-based TADF emitters, triphenylphosphine oxide (**TPPO)-tBu-DiKTa** and **TPA-tBu-DiKTa**, to address this problem (Figure 1). *Ortho*-substituted TPPO and TPA groups are introduced to increase the intermolecular distance and suppress ACQ. The electron-accepting TPPO group *ortho*-disposed to the nitrogen atom of the **DiKTa** core does not adversely affect the SRCT nature of the S_1 state of **TPPO-tBu-DiKTa**, which exhibits a narrow sky-blue emission at 472 nm (FWHM of 28 nm) in toluene. On the other hand, the presence of the *ortho*-linked electron-donating TPA group leads to new intramolecular charge transfer (CT) states resulting from π-stacking interactions between DiKTa and TPA for **TPA-tBu-DiKTa**. These states can become the lowest energy excited states in polar solvents. **TPA-tBu-DiKTa** emits at λ_{PL} of 481 nm and has a moderately broad emission (FWHM of 43 nm) in toluene. Both **TPPO-tBu-DiKTa** and **TPA-tBu-DiKTa** have high Φ_{PL} of 85% and 96% in 2 wt% doped films in mCP, respectively. In addition, there are no significant changes to the PL spectrum of **TPPO-tBu-DiKTa** at doping concentrations as high as 15 wt%, although the Φ_{PL} decreases to 63%, while for **TPA-tBu-DiKTa** the Φ_{PL} decreases to 76% and this is accompanied by a redshift in the emission. The OLEDs with 2 wt% of **TPPO-tBu-DiKTa** and 5 wt% of **TPA-tBu-DiKTa** showed EQE_{max} of 24.4% and 31.0%, respectively. The OLEDs with 10 wt% **TPA-tBu-DiKTa** not only exhibited comparably high EQE_{max} of 31.0% but also much reduced efficiency roll-off (EQE_{1000} of 20.4%). LECs based on the emitters dispersed into a blend-host:ionic liquid matrix exhibited narrowband blue emission with a FWHM of 35 nm. The optimized single-layer **TPA-tBu-DiKTa** LEC emitted blue light (λ_{EL} of 483 nm) with a luminance of 425 cd m^{-2} at an EQE_{max} of 2.6% and delivered a record-long operational lifetime for a MR-TADF-based LEC by the virtue of a relatively short delayed-fluorescence lifetime and a balanced electron and hole mobility.

2 | RESULTS AND DISCUSSION

2.1 | Synthesis

The synthesis of **TPPO-tBu-DiKTa** and **TPA-tBu-DiKTa** is outlined in Figure S1. **dBr-tBu-DiKTa** was obtained according to our previous work,[34] which was then converted into boronic ester **1** by palladium-catalyzed borylation with bis(pinacolato)diboron in 75% yield. This key intermediate was then reacted with **2** and **3** under Suzuki–Miyaura cross-coupling conditions to afford **TPPO-tBu-DiKTa** and **TPA-tBu-DiKTa** in 31% and 61% yield, respectively. Their identity and purity were characterized using melting point determination, ^{1}H- and ^{13}C-nuclear magnetic resonance (NMR) spectroscopy, high-resolution mass spectrometry (HRMS), high-performance liquid chromatography (HPLC), and element analysis. Both compounds are thermally stable as thermogravimetric analysis reveals high thermal decomposition temperatures (T_d, corresponding to 5% weight loss) of 466 and 452°C, respectively, for **TPPO-tBu-DiKTa** and **TPA-tBu-DiKTa**. No glass transition temperatures were observed from differential scanning calorimetry measurement (Figure S15).

2.2 | Theoretical calculations

The optimized geometries of the ground states and electronic structures of **TPPO-tBu-DiKTa** and **TPA-tBu-DiKTa** were calculated using density functional theory (DFT) at the PBE0/6-31G(d,p) level.[35,36] As shown in Figure 1, the LUMOs of both materials are localized on the **tBu-DiKTa** core. The HOMO of **TPPO-tBu-DiKTa** is also distributed on the **tBu-DiKTa** core. The calculated HOMO and LUMO energies of **TPPO-tBu-DiKTa** are −6.14/−2.32 eV. The electronic distribution and energy levels are similar to those of the parent compound **DiKTa** (−6.20/−2.23 eV).[16] By contrast, due to the strong electron-donating ability of the TPA moiety, the HOMO is localized on this fragment in **TPA-tBu-DiKTa** and the HOMO and LUMO energies are significantly destabilized compared to those of **TPPO-tBu-DiKTa** at −5.21 and −2.08 eV. The state energies and difference densities were calculated using spin-component scaling second-order algebraic diagrammatic construction (SCS-(ADC)2/cc-pVDZ) as this level of theory has been demonstrated to offer accurate predictions of the energies of the excited states transitions.[37,38] **TPPO-tBu-DiKTa** shows similar difference density patterns for both S_1 and T_1, localized on the **DiKTa** core that are characteristic of SRCT states. The S_1 and T_1 energies are 3.33 and 3.08 eV. For **TPA-tBu-DiKTa**, the difference density plot for the S_1 state resides on the **DiKTa** core, with a very small distribution on the N atoms of the TPA group, which indicates that this excited state possesses SRCT character. The S_1 and T_1 energies are 3.23 and 3.01 eV. The corresponding ΔE_{ST} values are calculated to be 0.25 and 0.22 eV for **TPPO-tBu-DiKTa** and **TPA-tBu-DiKTa**, respectively, which are of comparable magnitude to that of **DiKTa** (0.27 eV).[10]

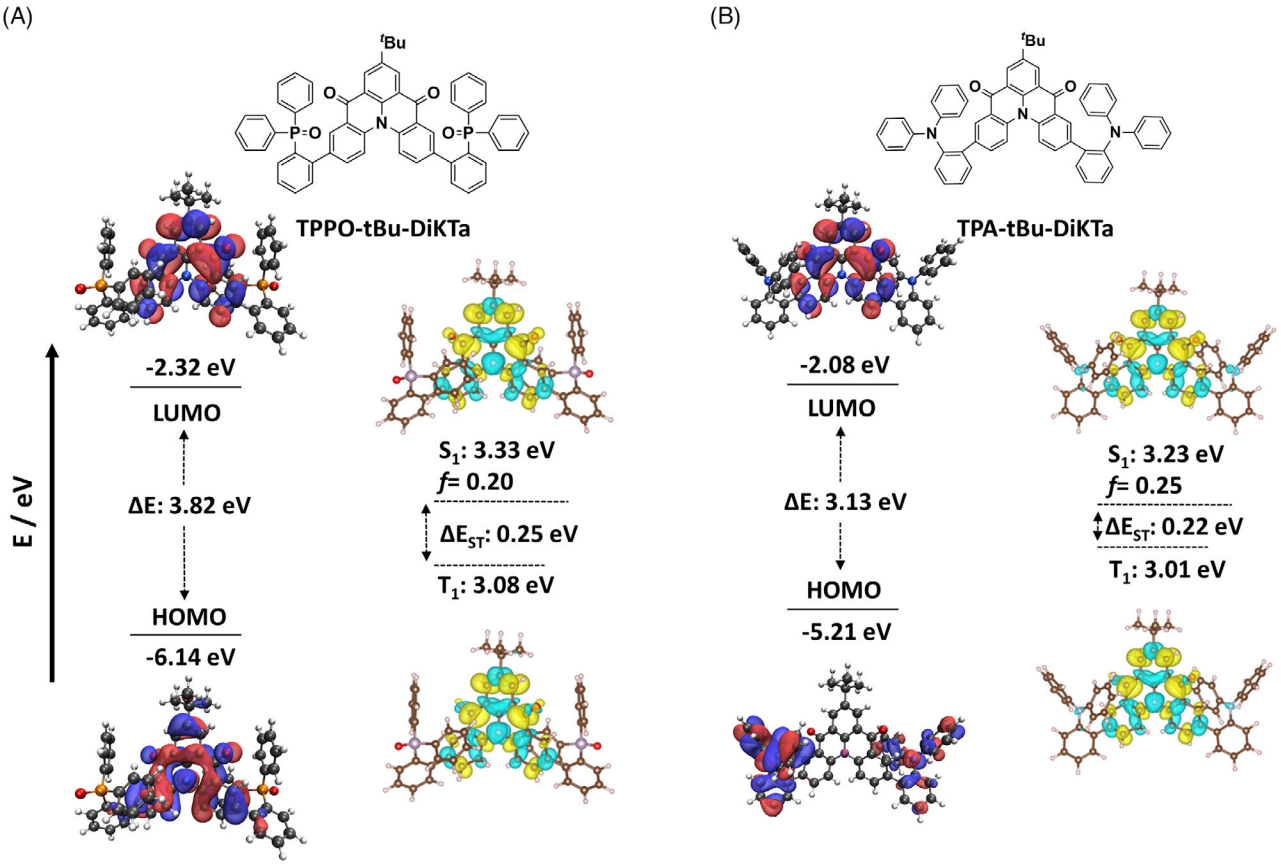

FIGURE 1 Chemical structures and calculated electron density distribution (isovalue: 0.02) of the highest occupied molecular orbital (HOMO), lowest unoccupied molecular orbital (LUMO), and orbital and state energy levels in the gas phase at the PBE0/6-31G(d,p) level, and difference density plots and energies of S_1 and T_1 calculated in the gas phase at spin-component scaling second-order algebraic diagrammatic construction (SCS-(ADC)2/cc-pVDZ) level, respectively, for (A) triphenylphosphine oxide (TPPO)-tBu-DiKTa and (B) triphenylamine (TPA)-tBu-DiKTa (blue indicates an area of decreased electron density while yellow indicates increased electronic density between the ground and excited states).

2.3 | Photophysical properties

We first investigated the ultraviolet–visible absorption and PL properties of **TPPO-tBu-DiKTa** and **TPA-tBu-DiKTa** in toluene at room temperature. As shown in Figure 2A, the absorption bands of **TPPO-tBu-DiKTa** and **TPA-tBu-DiKTa**, peaking at around λ_{abs} of 451 and 453 nm, are attributed to the SRCT S_0–S_1 absorption transitions.[16] The higher molar absorptivity of this band in **TPA-tBu-DiKTa** compared to that in **TPPO-tBu-DiKTa** is correlated to the higher calculated oscillator strength of the S_0–S_1 transition (0.20 for **TPPO-tBu-DiKTa** and 0.25 for **TPA-tBu-DiKTa**). The small bathochromic shifting of these bands compared to that of **DiKTa** (433 nm)[10] indicates that the peripheral groups weakly affect the electronic properties of the **DiKTa** core. **TPPO-tBu-DiKTa** and **TPA-tBu-DiKTa** both show narrowband emission at 472 and 481 nm, with FWHMs of 28 nm/0.16 eV and 43 nm/0.25 eV, respectively. The smaller Stokes shift and narrower emission for **TPPO-tBu-DiKTa** illustrate the smaller degree of geometry relaxation between ground and excited states in this compound.

To explore the nature of excited states of the two emitters, we performed a solvatochromism study by measuring the absorption and emission spectra in different solvents (Figures 2B,C, S16 and Tables S1 and S2). There is only a very small degree of positive solvatochromism observed for **TPPO-tBu-DiKTa**, which confirms that the emissive S_1 state has SRCT character. In contrast, **TPA-tBu-DiKTa** shows a SRCT-dominated emission in low polarity solvents; while, in higher polarity solvents, dual emission is observed as the LRCT state between the TPA donor and the **tBu-DiKTa** core becomes accessible and even lower in energy than the **tBu-DiKTa**-based SRCT state.[24] We have documented such behavior previously in donor-substituted DiKTa derivatives.[16] The relationship between the Stokes shift and solvent polarity was explored (Equations S1–S3).[39–41] As shown in Figure 2D, there is a single shallow slope in the Lippert–Mataga plot for **TPPO-tBu-DiKTa** that is consistent with an emissive SRCT excited state across all solvents. The Lippert–Mataga plot for **TPA-tBu-DiKTa** shows two regimes, indicative of different emissive excited states. In more polar solvents the emissive excited state possesses significant LRCT character whereas in less polar solvents the emissive excited state possesses SRCT character.

Fluorescence and phosphorescence spectra of **TPPO-tBu-DiKTa** and **TPA-tBu-DiKTa** in 2-methyltetrahydrofuran at 77 K were measured to extract the singlet and triplet energies and evaluate the ΔE_{ST} values (Figure S17). The singlet and triplet energies were determined from the onsets of the fluorescence and phosphorescence spectra, respectively. The calculated S_1 and T_1 energies for **TPPO-tBu-DiKTa** and **TPA-tBu-DiKTa** are 2.68/2.49 and 2.66/2.46 eV, respectively, resulting in moderate ΔE_{ST} values of 0.19 and 0.20 eV that are the same as that for **DiKTa** (0.20 eV)[10] and close to the calculated ones (0.25 and 0.22 eV). The absolute Φ_{PL} values of **TPPO-tBu-DiKTa** and **TPA-tBu-DiKTa** in degassed toluene are 47% and 50%, respectively. The time-resolved PL decays of the prompt emission in degassed toluene are shown in Figure 3A. The emission of **TPPO-tBu-DiKTa** decays with monoexponential kinetics with a lifetime (τ_{PL}) of 6.7 ns. No delayed emission was observed for **TPPO-tBu-DiKTa** in toluene, which is due in part to the moderately large ΔE_{ST} and the competing nonradiative decay processes with intersystem crossing (ISC)/RISC.[42] By contrast, the emission

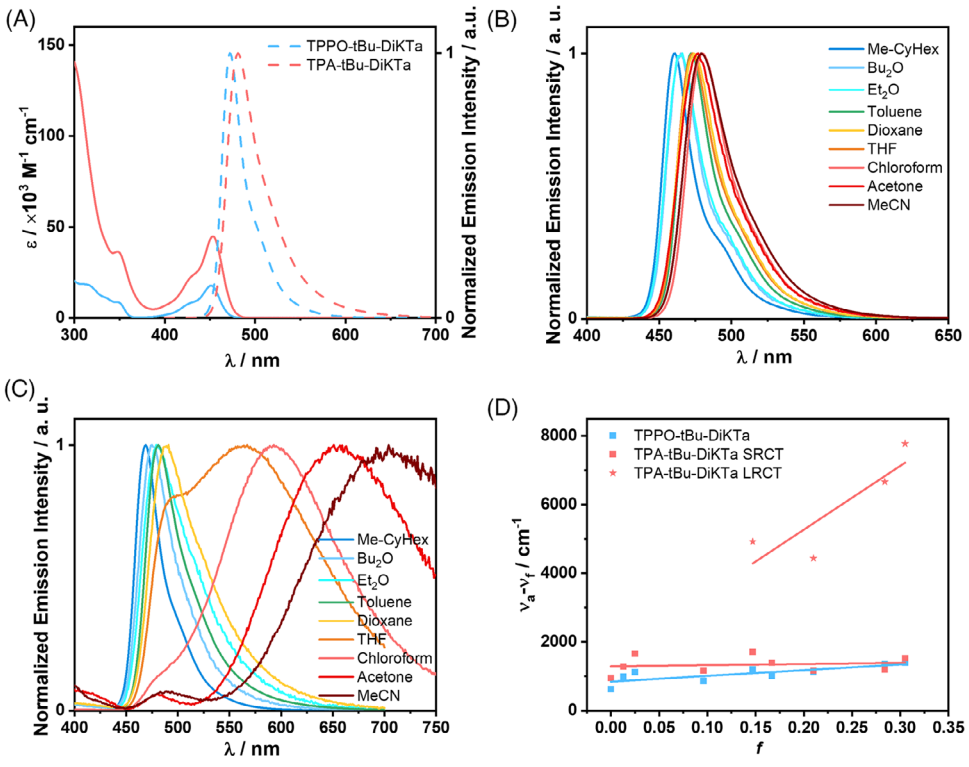

FIGURE 2 (A) Ultraviolet–visible (UV–vis) absorption spectra (solid lines) and photoluminescence (PL) spectra (dashed lines) of triphenylphosphine oxide **(TPPO)-tBu-DiKTa** and triphenylamine **(TPA)-tBu-DiKTa** in toluene at 300 K. PL spectra of (B) **TPPO-tBu-DiKTa** and (C) **TPA-tBu-DiKTa** in different solvents at 300 K (λ_{exc} = 340 nm). (D) Linear correlation of the Stokes shift with solvent orientational polarization (*f*) for **TPPO-tBu-DiKTa** and **TPA-tBu-DiKTa**. LRCT, long-range charge transfer; SRCT, short-range charge transfer; THF, tetrahydrofuran.

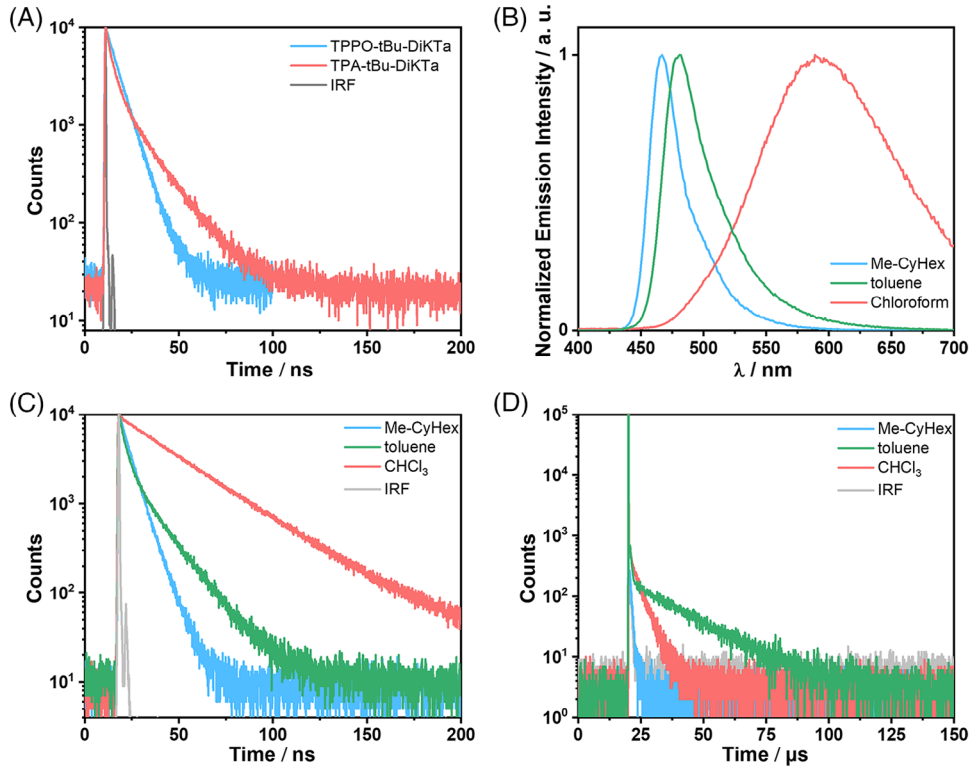

FIGURE 3 (A) Time-resolved photoluminescence (PL) of prompt emission in degassed toluene (λ_{exc} = 375 nm; IRF, instrument response function). (B) Steady-state PL of triphenylamine (TPA)-tBu-DiKTa in degassed methylcyclohexane (Me-CyHex), toluene, and chloroform (λ_{exc} = 340 nm). Time-resolved PL of (C) prompt emission (time window 0–200 ns) and (D) delayed emission (time window 0-150 μs) for TPA-tBu-DiKTa in degassed Me-CyHex, toluene and chloroform (λ_{exc} = 375 nm).

of **TPA-tBu-DiKTa** decays with multiexponential kinetics, with prompt lifetimes, τ_p, of 3.2 and 14 ns and a delayed lifetime, τ_d, of 18 μs (Figure 3D). The additional longer prompt and delayed lifetime components of **TPA-tBu-DiKTa** compared to **TPPO-tBu-DiKTa** may originate from the radiative decay from the LRCT state, which would have a lower oscillator strength and thus a slower radiative decay rate, k_r, than that from the SRCT state. The presence of a low-lying LRCT state may result in smaller ΔE_{ST}, which facilitates the RISC process. To verify this hypothesis, steady-state PL spectra and time-resolved PL decays of **TPA-tBu-DiKTa** in degassed methylcyclohexane (Me-CyHex) and chloroform were also measured (Figure 3B–D). In the nonpolar Me-CyHex, the emission is both bluer and narrower (λ_{PL} = 467 nm; FWHM of 30 nm), with a fast τ_p of 6.2 ns and no observed delayed emission, which is similar to the photophysical behavior of **TPPO-tBu-DiKTa**, implying emission from a SRCT state. In higher polarity chloroform, the emission is much redder and broader (λ_{PL} = 589 nm; FWHM of 132 nm). The time-resolved PL decay has a longer τ_p of 30 ns and a shorter τ_d of 3.7 μs than in toluene, which is typical for emission from a LRCT state emblematic of D–A TADF emitters. The change in photophysical behavior as a function of solvent polarity confirms the presence of two different CT states, where the LRCT state becomes the lowest in energy in more polar media. In the moderate polarity solvents such as toluene, the SRCT and LRCT states are relatively close in energy, thus making it possible to detect both SRCT and LRCT emission.

The propensity for these two compounds to aggregate and show aggregation-induced emission (AIE) was investigated across a series of tetrahydrofuran/water solutions with increasing water content.[43] As shown in Figure S18, with the increase of water fraction (f_w) from 0% to 90%, the emission intensity of **TPPO-tBu-DiKTa** progressively drops as the emission redshifts, which is linked to a progressively stabilized emissive CT state with increasing polarity; thus, this compound does not show AIE. By contrast, the emission intensity of **TPA-tBu-DiKTa** decreases first when the f_w increases from 0% to 60% but then increases significantly and the spectra blueshift from 588 to 564 nm when the f_w is higher than 60%, which indicates that **TPA-tBu-DiKTa** shows AIE behavior, meaning that there is a strong suppression of nonradiative decay in the aggregated state.[44,45]

With a view to exploiting these materials as emitters for OLEDs, the photophysical properties of films were then investigated. mCP was used as the host material because of its suitably high triplet energy (2.9 eV).[46] The absolute Φ_{PL} values of TPPO-tBu-DiKTa and TPA-tBu-DiKTa at different doping concentrations in mCP were measured under a nitrogen atmosphere (Table S3). Due to the suppressed nonradiative decay in the rigid matrix and the interaction between host and guest materials,[42] the Φ_{PL} values in mCP films are higher than those in dilute toluene. TPPO-tBu-DiKTa and TPA-tBu-DiKTa have the highest Φ_{PL} value of 85% and 96% in 2 wt% doped films in mCP; indeed, the Φ_{PL} of the 1, 5, 10, and 15 wt% doped films of TPPO-tBu-DiKTa in mCP progressively decrease from 84% to 73%, 67%, and 63% without any major changes to the PL spectra (Figure S20A). For TPA-tBu-DiKTa, the Φ_{PL} is 93% and 96% for the 1 and 5 wt% doped films in mCP, while the value decreases to 83% for the 10 wt% doped films. When increasing the doping concentrations to 15 and 25 wt%, the emission broadens and redshifts while the Φ_{PL} decreases to 76% and 73%, respectively (Figure S20C). Contributions

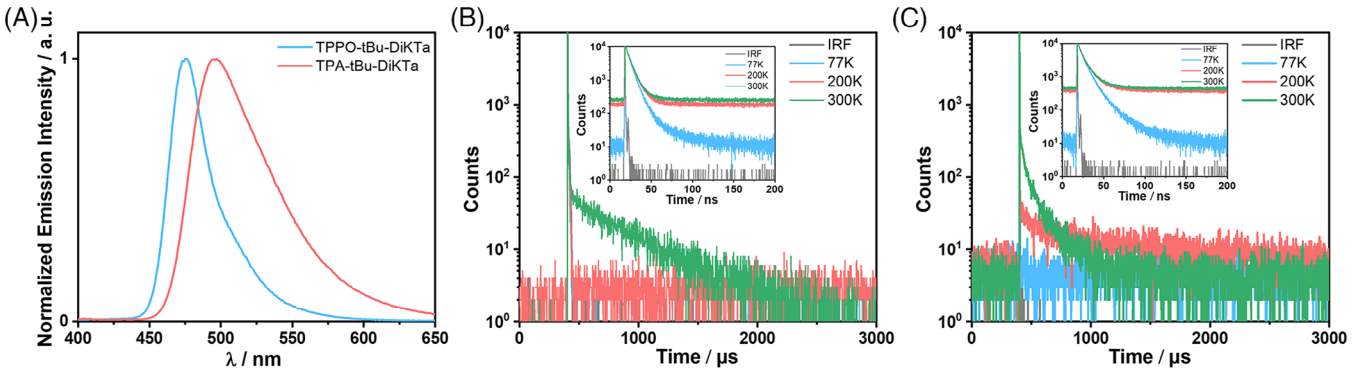

FIGURE 4 (A) Steady-state photoluminescence (PL) spectra at 300 K in 2 wt% doped films in 1,3-bis(*N*-carbazolyl) benzene (mCP; λ_{exc} = 340 nm). Temperature-dependent time-resolved PL decays of (B) triphenylphosphine oxide (TPPO)-tBu-DiKTa and (C) triphenylamine (TPA)-tBu-DiKTa in 2 wt% doped films in mCP (inset figures are PL decays of prompt components; λ_{exc} = 375 nm; IRF, instrument response function).

from intermolecular CT states cannot be ruled out. Compared to the larger decreases of the reported Φ_{PL} for DiKTa (51%, 37%, and 16% in 1, 5, and 10 wt% doped films in mCP) and Mes_3DiKTa (52%, 38%, 42%, and 26% in 3.5, 5, 10, and 20 wt% doped films in mCP),[10] the generally higher absolute values and smaller decreases in Φ_{PL} for **TPPO-tBu-DiKTa** and **TPA-tBu-DiKTa** illustrate clearly that the *ortho*-substituted groups help to suppress ACQ.

Steady-state PL spectra of the 2 wt% doped films in mCP were first investigated because of their highest Φ_{PL} (Figure 4A). **TPPO-tBu-DiKTa** and **TPA-tBu-DiKTa** show blue and green emission at 476 nm (FWHM of 34 nm/0.19 eV) and 497 nm (FWHM of 64 nm/0.34 eV), respectively. The redshifted emission compared with the spectra in toluene for both emitter (λ_{PL} = 472 nm, FWHM = 28 nm/0.16 eV for **TPPO-tBu-DiKTa** and λ_{PL} = 481 nm, FWHM = 43 nm/0.25 eV for **TPA-tBu-DiKTa**) is ascribed to explicit host–guest interactions.[42] The relatively broader emission band of **TPA-tBu-DiKTa** may result from the intermolecular interaction between TPA and DiKTa moieties between different guest molecules. The temperature-dependent time-resolved PL decays under vacuum are shown in Figure 4B–E. **TPPO-tBu-DiKTa** shows a fast τ_p of 6.5 ns and due to the suppressed nonradiative decay in the rigid matrix, the RISC process becomes detectable and a long τ_d of 432 μs is observed at 300 K. **TPA-tBu-DiKTa** shows both double-exponential prompt and delayed components, with τ_p of 5.2 and 13 ns, and τ_d of 30 and 177 μs. The intermolecular interactions between host–guest and guest–guest cannot be avoided in the film state, which is different from the properties of isolated molecules in dilute solution. Together with the progressive redshifting of the PL spectra in films with increased **TPA-tBu-DiKTa** doping concentration (Figure S20C), the longer prompt and shorter delayed lifetime components may mainly originate from intermolecular CT states rather than the intramolecular CT state that influences the photophysics in isolated molecules. Both emitters display temperature insensitive prompt fluorescence and thermally activated delayed emission spectra from 77 to 300 K, which confirm that in mCP these two compounds are TADF emitters. The photophysical kinetics parameters for the 2 wt% doped films are summarized in Table S4. The rate constant for RISC (k_{RISC}) is 4.0 × 10^3 s^{-1} for **TPPO-tBu-DiKTa**, which is close to that of the previously reported **Mes_3DiKTa** (k_{RISC} of 3.1 × 10^3 s^{-1})[47] and somewhat slower than that of **DiKTa** (k_{RISC} of 2.5 × 10^4 s^{-1}).[27] A possible explanation to these relative k_{RISC} values is that the bulky TPPO groups to some extent inhibit exciplex-like interactions between **TPPO-tBu-DiKTa** and mCP, which have been shown to accelerate ISC and RISC.[42] k_{RISC} is calculated to be 1.8 × 10^4 s^{-1} for **TPA-tBu-DiKTa**, which is more than four times faster than that of **TPPO-tBu-DiKTa**. This improvement indicates that the contributions from intermolecular CT states in the film may also help improve RISC. As bipolar cohost systems are frequently used in OLEDs, we also checked their properties in 2 wt% doped films in a mCP: 2,8-bis(diphenyl-phosphoryl)-dibenzo[b,d] thiophene (PPT) cohost (Figure S19). The data are summarized in Table S5.

Time-resolved PL decays of **TPPO-tBu-DiKTa** and **TPA-tBu-DiKTa** at higher doping concentrations were also measured. As shown in Figure S20B,D and Table S6, the τ_d of **TPPO-tBu-DiKTa** remains similar in the 5, 10, and 15 wt% doped films at 392, 392, and 372 μs, leading to k_{RISC} of 3.8 × 10^3, 4.3 × 10^3, and 5.4 × 10^3 s^{-1}, respectively. This means that higher doping concentrations will not adversely affect the kinetics of the TADF. The lifetime behavior of **TPA-tBu-DiKTa** is similar for the 5 and 10 wt% doped films, with τ_d of 26/176 μs and 13/147 μs and k_{RISC} of 1.9 × 10^4 and 1.6 × 10^4 s^{-1}, respectively. However, as 15 and 25 wt% doped films, a low-lying CT emission distinct from the monomolecular SRCT emission becomes dominant (Figure S20C), assigned as an intermolecular CT. As a result, TADF becomes more efficient, reflected in the shorter τ_d of 12/80 μs and 8.6/60 μs and faster k_{RISC} of 4.1 × 10^4 and 4.5 × 10^4 s^{-1}, respectively. These results indicate that both **TPPO-tBu-DiKTa** and **TPA-tBu-DiKTa** are suitable for use at high doping concentrations in the emissive layer of electroluminescent devices.

2.4 | Electrochemistry

The electrochemical properties of **TPPO-tBu-DiKTa** and **TPA-tBu-DiKTa** were investigated by cyclic voltammetry (CV) and differential pulse voltammetry (DPV) in degassed dichloromethane (DCM) with 0.1 M [^{n}Bu_4N]PF_6 as the supporting electrolyte and Fc/Fc^+ as the internal reference (0.46 V vs. saturated calomel electrode, SCE)[48] in order to estimate the HOMO and LUMO values. As shown in Figure S21, there is an irreversible oxidation wave for

TPPO-tBu-DiKTa at an oxidation potential, E_{ox} of 1.80 V versus SCE, which is consistent with the E_{ox} of **DiKTa** at 1.78 V,[16] indicating that the HOMO is localized on the **tBu-DiKTa** core. By contrast, there is a reversible oxidation wave that is cathodically shifted to 1.04 V for **TPA-tBu-DiKTa**, which is similar to that of **3TPA-DiKTa** at 0.93 V[20] and is assigned to oxidation of the TPA group. The CVs of both compounds show reversible reduction waves, with reduction potentials (E_{red}) from the DPV of −1.41 and −1.45 V, respectively, which are close to that of **DiKTa** at −1.34 V.[16] The corresponding HOMO and LUMO energies of **TPPO-tBu-DiKTa** and **TPA-tBu-DiKTa** are calculated to be −6.14/−2.93 and −5.38/−2.89 eV with ΔE of 3.21 and 2.49 eV, respectively. These trends align with the DFT calculations (−6.14/−2.32 eV and −5.21/−2.08 eV, respectively). The data are summarized in Table S7.

2.5 | Organic light-emitting diodes

Given their high Φ_{PL} in mCP films, we next proceeded to fabricate vacuum-deposited OLEDs. The OLED device stack and the chemical structures of the organic layers are shown in Figure 5A,B. The OLED device structure

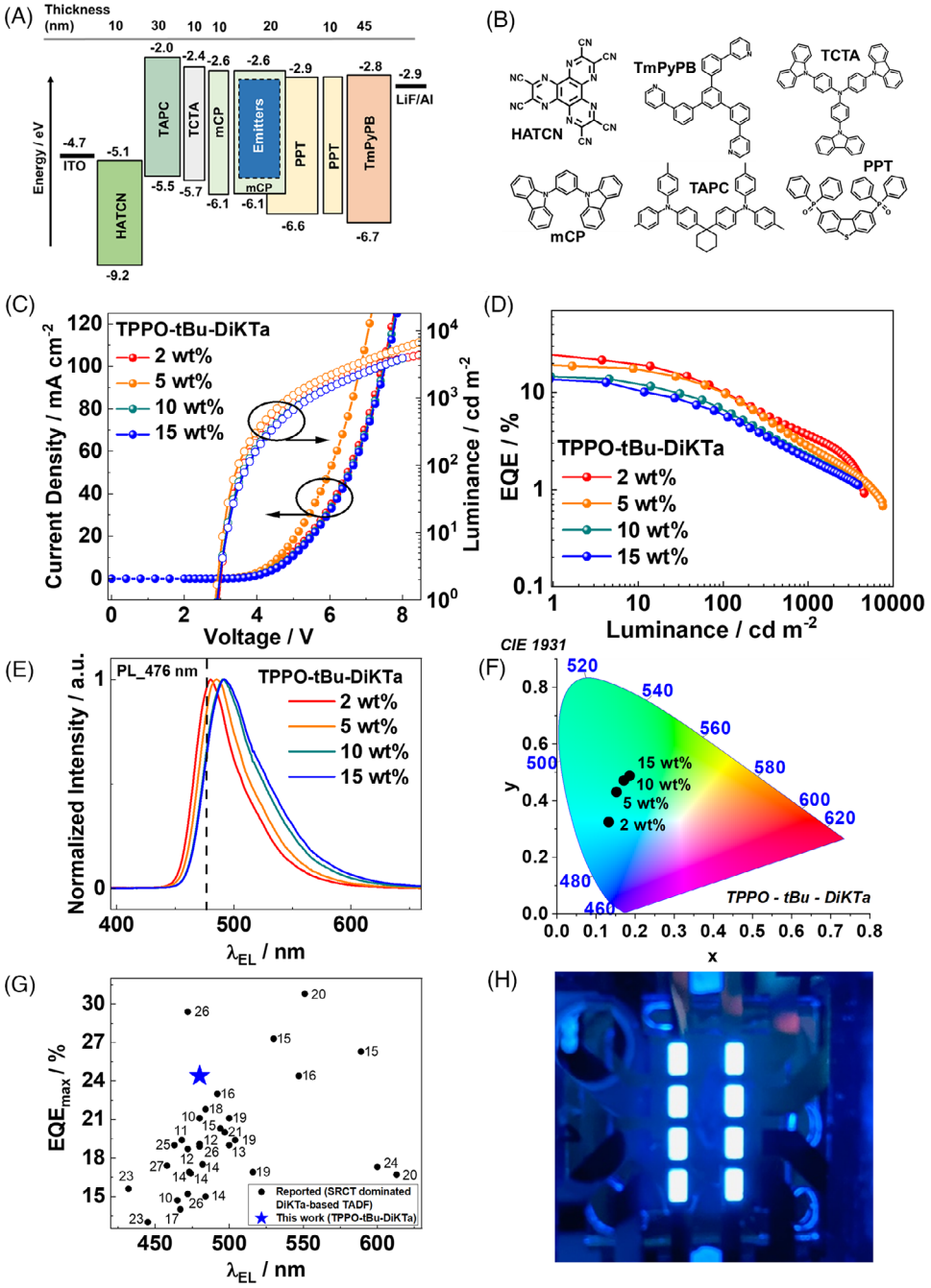

FIGURE 5 (A) Schematic of the device stack of the organic light-emitting diodes (OLEDs). (B) Chemical structures of the organic layers. (C–F) OLED device performance for triphenylphosphine oxide (TPPO)-tBu-DiKTa with 2, 5, 10, 15 wt% of the emitter. (C) Current density–voltage–luminescence (JVL) characteristics. (D) External quantum efficiency (EQE) versus luminescence. (E) Electroluminescence (EL) spectra. (F) Commission International de l'Éclairage (CIE) coordinates for the OLEDs. (G) EQE_{max} versus λ_{EL} comparison for reported multiresonant thermally activated delayed fluorescence (MR-TADF) DiKTa-based OLEDs[10–27] with TPPO-tBu-DiKTa (labels show the references for the respective data points, chemical structures, and device data are provided in Figure S23 and Table S10, respectively). (H) Photograph of the OLEDs fabricated with 2 wt% TPPO-tBu-DiKTa. HATCN, 1,4,5,8,9,11-hexaazatriphenylenehexacarbonitrile; mCP, 1,3-bis(*N*-carbazolyl) benzene; PPT, 2,8-bis(diphenyl-phosphoryl)-dibenzo[b,d] thiophene; TAPC, 1,1-bis[(di-4-tolylamino)phenyl]cyclohexane; TCTA, tris(4-carbazoyl-9-ylphenyl)amine; TmPyPB, 1,3,5-tris(3-pyridyl-3-phenyl)benzene.

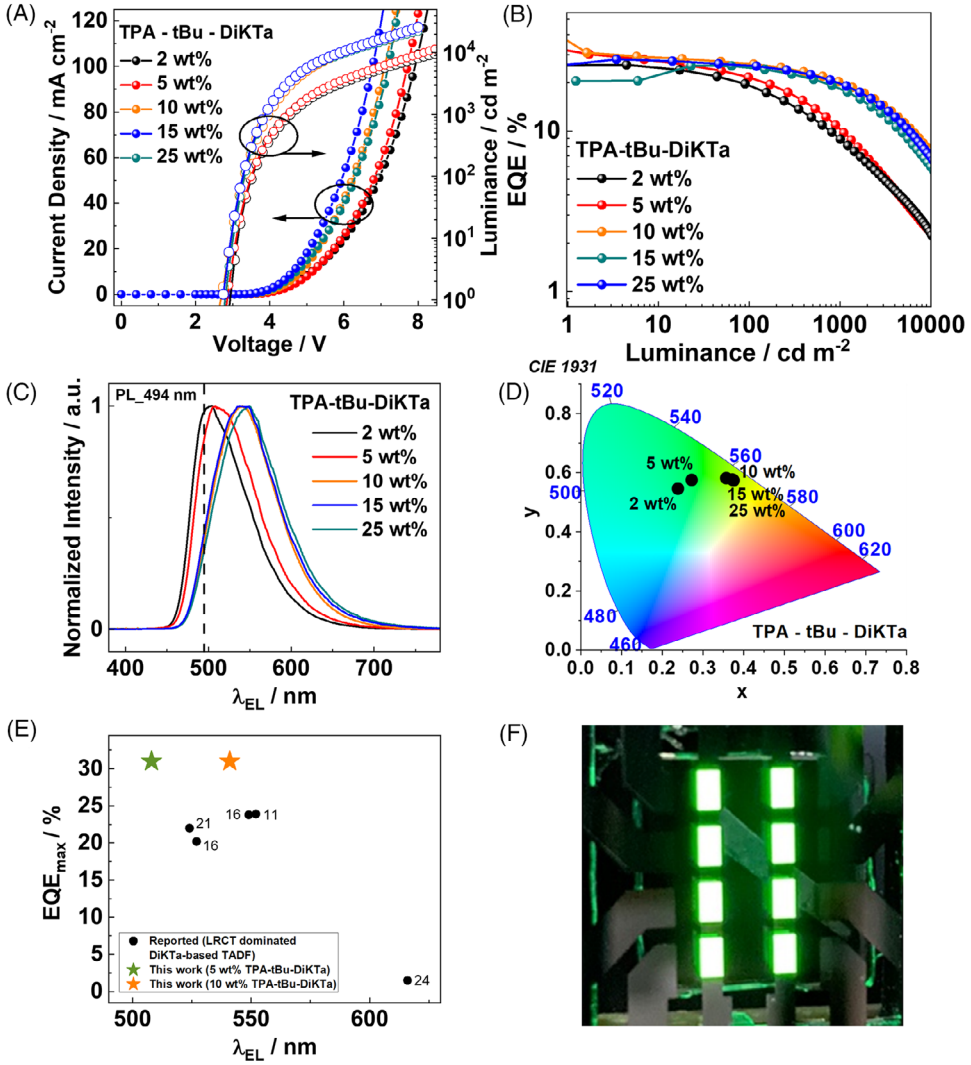

FIGURE 6 Organic light-emitting diodes (OLEDs) device performance for triphenylamine (TPA)-tBu-DiKTa with 2, 5, 10, 15, and 25 wt% of the emitter. (A) Current density–voltage–luminescence (JVL) characteristics. (B) External quantum efficiency (EQE) versus luminescence. (C) Electroluminescence (EL) spectra. (D) Commission International de l'Éclairage (CIE) coordinates for the OLEDs. (E) EQE_{max} versus λ_{EL} comparison for reported long-range charge transfer (LRCT)-dominated DiKTa-based thermally activated delayed fluorescence (TADF) OLEDs[11,16,21,24] with TPA-tBu-DiKTa (labels show the references for the respective data points, chemical structures, and device data are provided in Figure S24 and Table S10, respectively). (F) Photograph of the OLEDs fabricated with 2 wt% of TPA-tBu-DiKTa.

consisted of: indium tin oxide (ITO)/1,4,5,8,9,11-hexaazatriphenylenehexacarbonitrile (HATCN, 10 nm)/1,1-bis[(di-4-tolylamino)phenyl]cyclohexane (TAPC, 30 nm)/tris(4-carbazoyl-9-ylphenyl)amine (TCTA, 10 nm)/mCP (10 nm)/mCP:PPT as cohost (20 nm) with **TPPO-tBu-DiKTa,** and **TPA-tBu-DiKTa** as emitter dopants/PPT (10 nm)/1,3,5-tris(3-pyridyl-3-phenyl)benzene (TmPyPB, 45 nm)/lithium fluoride (LiF, 0.8 nm)/aluminum (Al, 100 nm). Here, HATCN was used as the hole injection layer, TAPC as the hole transporting layer, TCTA as a combined hole transporting and electron blocking layer, mCP as an exciton blocking layer, PPT as a hole blocking layer, TmPyPB as an electron transporting layer, and LiF was used to reduce the work function of the top Al electrode. The mCP:PPT cohost system used in the devices was chosen to facilitate the mobility of both charge carriers in the EML and to broaden the recombination zone, which should lead to a decrease in bimolecular exciton quenching pathways by reducing the triplet density.[27]

The device performance of the OLEDs at various concentrations (2, 5, 10, 15 wt%) of **TPPO-tBu-DiKTa** as an emitter is shown in Figure 5. The current density–voltage–luminescence (JVL) characteristics of the devices (Figure 5C) all showed a low turn-on voltage of 2.9 V for all concentrations of the emitter. An EQE_{max} of 24.4% was obtained using 2 wt% of **TPPO-tBu-DiKTa** (Figure 5D) with a drop in EQE to 10.0% at 100 cd m^{-2} (EQE_{100}). The devices showed blue EL at λ_{EL} of 480 nm (Figure 5E), which is close to the PL emission in mCP at 476 nm for this emitter (Figure 4). However, the FWHM of the EL spectrum was slightly wider (46 nm) than that of the PL spectrum (34 nm), which may be due to the differences in polarity of the cohost system compared to mCP. The Commission International de l'Éclairage, CIE, coordinates (Figure 5F) for the 2 wt% **TPPO-tBu-DiKTa** devices were (0.133, 0.323). With increase in concentration of the emitter to 5 wt% the EQE_{max} dropped to 18.8% and continued to decrease for 10 and 15 wt% doping of the emitter to 14.6% and 13.7%, respectively. This decrease in efficiency is consistent with the progressively lower Φ_{PL} observed for **TPPO-tBu-DiKTa**, which decreased from 85% (for 2 wt% doped films) to 63% (for 15 wt% doped films). There is a slight redshift and

broadening of the EL spectra of the OLEDs with increasing doping concentration (Figure 5E). The comparison between the EQE_{max} of the OLEDs with **TPPO-tBu-DiKTa** and other DiKTa-based MR-TADF OLEDs in the literature (Figure 5G) highlights the particularly high EQE_{max} especially in the λ_{EL} range of 450–525 nm. The photograph of the OLEDs with 2 wt% **TPPO-tBu-DiKTa** is shown in Figure 5H.

OLEDs were also fabricated with **TPA-tBu-DiKTa** with 2, 5, 10, 15, and 25 wt% concentrations using the same device structure. The JVL curves of the devices (Figure 6A) show a higher current density and luminance for the 10, 15, and 25 wt% than for 2 and 5 wt%. An impressive EQE_{max} of 31% (Figure 6B) was achieved using 5 wt% of **TPA-tBu-DiKTa**, which drops to 21.8% at 100 cd m^{-2} and 11% at 1000 cd m^{-2}. The 5 wt% device emitted at λ_{EL} of 508 nm (Figure 6C), which is close to the λ_{PL} of 497 nm (Figure 4); the corresponding CIE coordinates (Figure 6D) are (0.27, 0.57). When the concentration of the emitter was increased to 10 wt%, not only was the EQE_{max} of 31.0% retained despite the lower Φ_{PL} of 83% at this doping concentration, but also the efficiency roll-off was considerably decreased, with an EQE_{100} of 26.4% and EQE_{1000} of 20.4%. The high EQE_{max} at higher emitter concentrations is a strong indicator that the improved **TPA-tBu-DiKTa** emitter design reduces ACQ. The improved EQE_{max} for the device with **TPA-tBu-DiKTa** as compared to that with **TPPO-tBu-DiKTa** is also coherent with the higher Φ_{PL} of the former at all doping concentrations. The reduced efficiency roll-off of the 10 wt% doped device with **TPA-tBu-DiKTa** (34.2% at 1000 cd m^{-2}) compared to that of the 5 wt% doped devices with **TPA-tBu-DiKTa** (64.5% at 1000 cd m^{-2}) and the 2 wt% doped devices with **TPPO-tBu-DiKTa** (85.2% at 1000 cd m^{-2}) aligns with the faster k_{RISC} and shorter τ_d in **TPA-tBu-DiKTa** as a result of the presence of low-lying intermolecular CT states in this emitter. The EL of the devices with greater than 10 wt% emitter doping concentration was significantly redshifted to 541 nm and slightly broadened from a FWHM of 77 nm (2 wt%) to 84 nm (10 wt%). This is in accordance with the shifts in the PL spectra observed for the higher concentrations of **TPA-tBu-DiKTa** (Figure S20C) and might be attributed to the emission from intermolecular CT states. The devices fabricated using even higher emitter doping concentrations (15 and 25 wt%) showed similarly high EQE_{max} and lower efficiency roll-off than those with 10 wt% emitter doping (Figure 6B). This implies that both the ACQ, and bimolecular quenching processes (such as S–T and T–T annihilation) are considerably suppressed in these devices. The particularly high EQE_{max} suggests that the transition dipole moment (TDM) of **TPA-tBu-DiKTa** may be preferentially horizontally oriented. We thus investigated the orientation of the TDM emitter by making angle-dependent PL measurements on 5 wt% of **TPA-tBu-DiKTa** emitter in mCP:PPT cohost (Figure S22). The study implies that the TDM of **TPA-tBu-DiKTa** is indeed preferentially horizontally oriented with a ratio (Θ) of 72.5%. This implies an improved light outcoupling efficiency that contributes to the high overall EQE_{max} of the devices as compared to devices with emitters that are almost randomly oriented, having lower Θ (62%).[49] The EQE_{max} of the OLEDs with **TPA-tBu-DiKTa** was higher than literature examples of devices with **DiKTa**-based TADF emitters showing EL from a LRCT state (Figure 6E). A photograph of a 2 wt% **TPA-tBu-DiKTa** OLEDs is shown in Figure 6F.

2.6 | Light-emitting electrochemical cells

A LEC comprises, by definition, mobile ions in its active material.[50] In functional LECs, the external bias-induced redistribution of these ions results in injection-facilitating electric double layer (EDL) formation at the two electrode/active-material interfaces, followed by electrochemical doping of the luminescent organic semiconductor(s) in the active material; n-type at the negative cathode and p-type at the positive anode. The latter process concludes with the in situ formation of a p–n junction doping structure in the active material.[51,52] This intricate turn-on process enables LEC architectures that consist of solely air-stable and solution-processable materials, and it has been shown that such robust LEC devices can be fabricated by noninterrupted ambient-air printing and coating.[53,54]

This opportunity for material- and energy-efficient fabrication is desirable for cost-sensitive and sustainable electroluminescent devices, but it should be noted that the LEC performance is strongly dependent on the merits and combined function of the luminescent semiconductor and the mobile ions. For instance, it has recently been demonstrated that MR-TADF compounds can function as the luminescent organic semiconductor in LEC devices,[4,22,32,33] but also that the propensity for ACQ can be highly detrimental to both the LEC-critical ion redistribution process and the emission efficiency.[45] It is thus interesting and timely to investigate and compare the performance of LECs employing **TPA-tBu-DiKTa** and **TPPO-tBu-DiKTa**.

The LECs were fabricated by spin coating the active material on a transparent ITO/poly(3,4-ethylenedioxythiophene)-poly(styrenesulfonate (PEDOT:PSS) anode, with the top cathode being reflective Al. The selected source of mobile ions was the ionic liquid, tetrahexylammonium tetrafluoroborate ($THABF_4$), and its concentration in the active material was 10 wt%. The ITO/PEDOT:PSS/active-material/Al devices were driven at a constant current density of 7.7 mA cm^{-2}. We established that both **TPPO-tBu-DiKTa** and **TPA-tBu-DiKTa** exhibit a high solubility (>40 g L^{-1}) in chlorobenzene, and that it accordingly was possible to spin-coat uniform pinhole-free films from the MR-TADF:ionic liquid blend. These thin films were investigated for the active material in "host-free" LECs, but the performance of these devices was very poor (see Table S8), because of ACQ-hindered ion mobility and ACQ-induced exciton quenching.

We thus attempted to disperse **TPPO-tBu-DiKTa** and **TPA-tBu-DiKTa** in a host matrix in the form of either 26DCzPPy, 26DCzPPy:TCTA, or 26DCzPPy:PYD2Cz. We found that the inclusion of 26DCzPPy was necessary in order to form uniform and pinhole-free host:guest:ionic liquid "active-material" films by solution processing. Figure 7A shows that the spectral overlap between the PL spectra of neat films of the three host matrices and the absorption spectrum of the dilute solutions of the two emitters is relatively strong. All six different host:guest combinations thus fulfill a basic

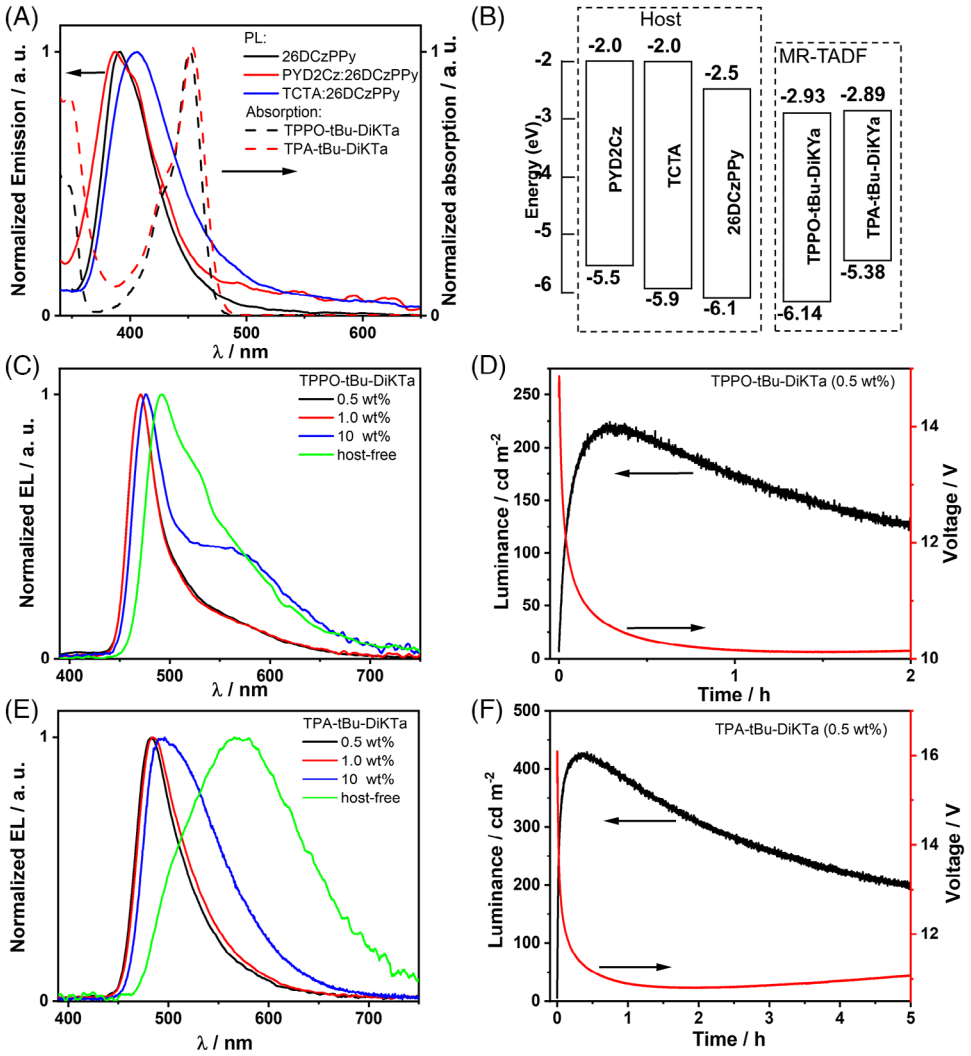

FIGURE 7 (A) The normalized photoluminescence (PL) spectra of the three host systems in film form (solid lines) and the normalized absorption spectra of the two multiresonant thermally activated delayed fluorescence (MR-TADF) emitters in dilute toluene solution (dashed lines). (B) The electron–energy diagram of the three host compounds (left) and the two MR-TADF emitters (right). (C) The normalized electroluminescence (EL) spectra for 0.5, 1.0, 10 wt% and host-free triphenylphosphine oxide (TPPO)-tBu-DiKTa light-emitting electrochemical cells (LECs). (D) The temporal evolution of the luminance (left *y*-axis) and the voltage (right *y*-axis) of the 0.5 wt% TPPO-tBu-DiKTa LEC. (E) The normalized EL spectra for 0.5, 1.0, 10 wt% and host-free triphenylamine (TPA)-tBu-DiKTa LECs. (F) The temporal evolution of the luminance (left *y*-axis) and the voltage (right *y*-axis) of the 0.5 wt% TPA-tBu-DiKTa LEC. The LEC devices in (C–F) were driven by a constant current density of 7.7 mA cm^{-2}.

requirement for Förster resonance energy transfer from the host matrix to the guest. Table S9 further reveals that the three hosts exhibit a higher triplet energy than the emitters, which facilitates efficient host-to-guest energy transfer by the Dexter mechanism. The electron–energy structure depicted in Figure 7B finally indicates that both the electrons and holes will be trapped on the guest emitter in the three host:**TPA-tBu-DiKTa** systems, whereas it is solely the electrons that are efficiently trapped in the three host:**TPPO-tBu-DiKTa** systems.

We have systematically investigated the performance of the ITO/PEDOT:PSS/host:guest:$THABF_4$/Al LECs as a function of the host selection and the guest emitter concentration, and Table S8 shows that the best performance is invariably attained with the host being 26DCzPPy:TCTA and the guest concentration being 0.5 wt%. Figure 7C shows that a narrowband EL spectrum, with a FWHM of 35 nm, can be delivered from the 26DCzPPy:TCTA:**TPPO-tBu-DiKTa** LEC for a guest emitter concentration of either 0.5 or 1.0 wt%, but that a higher guest concentration results in a broadened emission envelope.

Importantly, Figure 7D shows that the luminance increases, and the voltage decreases, with time during the initial operation of a pristine 26DCzPPy:TCTA:**TPPO-tBu-DiKTa** LEC, which is in line with that the ions are mobile in the active material and can enable the desired formations of EDLs and a p–n junction doping structure. This LEC device, which comprised optimized values for the guest emitter concentration of 0.5 wt% and the 26DCzPPy:TCTA ratio of 5:3, did not only deliver narrowband emission but also a respectable EQE_{max} of 1.6%. However, the best device performance was obtained with the **TPA-tBu-DiKTa** LEC. It also delivered ACQ-free emission at low guest concentration (see Figure 7E), as well as the classic signature of LEC operation in the form of increasing luminance and decreasing voltage during the initial constant-current operation (Figure 7F). However, the emission efficiency and the operational stability was significantly improved compared to the **TPPO-tBu-DiKTa** LEC, as manifested in an EQE_{max} of 2.6% and an operational stability above 100 cd m^{-2} of 15 h (compared to 3 h for the **TPPO-tBu-DiKTa** LEC, see Table S8).

TABLE 1 Photophysical data of triphenylphosphine oxide **(TPPO)-tBu-DiKTa** and triphenylamine **(TPA)-tBu-DiKTa**.

Compound	λ_{abs}[a]/nm	λ_{PL}[a] (FWHM)/nm	Φ_{PL}[a]/%	λ_{PL}[b] (FWHM)/nm	Φ_{PL}[b]/%	ΔE_{ST}[c]/eV	τ_p[b]/ns	τ_d[b]/μs
TPPO-tBu-DiKTa	451	472 (28)	47	476 (34)	85	0.19	6.5	432
TPA-tBu-DiKTa	453	481 (43)	50	497 (64)	96	0.20	5.2, 13	30, 177

Abbreviation: FWHM, full width at half maximum.
[a]Measured in toluene solution.
[b]Measured in 2 wt% doped 1,3-bis(*N*-carbazolyl) benzene (mCP) films.
[c]Measured in 2-methyltetrahydrofuran (2-MeTHF) solution.

The origin of the better performance of the **TPA-tBu-DiKTa** LECs warrants a discussion. We first note that the Φ_{PL} of the two optimized active-material films is essentially identical at 76%–78%, and that the capacity for host-to-guest energy transfer by both the Förster and Dexter processes appear to be similar based on the presented data. However, we do recognize that previous LEC studies have demonstrated that detrimental exciton–polaron quenching can be alleviated by a balancing of the electron and hole transport within the active material.[55,56] In this context, we note that **TPPO-tBu-DiKTa** forms electron but not hole traps in the 26DCzPPy:TCTA matrix, whereas **TPA-tBu-DiKTa** forms both electron and hole traps (Figure 7B). It is thus reasonable that a non-balanced mobility (specifically a much higher hole than electron mobility) will prevail in the **TPPO-tBu-DiKTa** LEC, which is comparatively more balanced in the **TPA-tBu-DiKTa** LEC. In line with the earlier findings, this would thus explain the higher EQE_{max}. The significantly improved operational stability of the **TPA-tBu-DiKTa** LECs can be attributed to the shorter value of τ_d (Table 1), which will mitigate both exciton–exciton and exciton–polaron quenching and related deleterious side reactions. In this context, we mention that the measured operational lifetime of the optimized **TPA-tBu-DiKTa** LEC represents an improvement by a factor of 5 compared to the state-of-the-art[33] in the MR-TADF LEC field.

3 | CONCLUSIONS

Two new MR-TADF emitters **TPPO-tBu-DiKTa** and **TPA-tBu-DiKTa** have been designed and synthesized. The SCS-(ADC)2 calculations and photophysical property study indicate that the emissive excited state for both **TPPO-tBu-DiKTa** and **TPA-tBu-DiKTa** is of SRCT character. For **TPA-tBu-DiKTa**, there are contributions from intermolecular CT states that result in an accelerated RISC process (k_{RISC} of 1.8×10^4 s^{-1} in 2 wt% doped film in mCP when compared with k_{RISC} of 4.0×10^3 s^{-1} for **TPPO-tBu-DiKTa**). The twisted *ortho*-substituted geometries suppress the aggregation between DiKTa moieties and alleviate the ACQ of emitters in films even at high doping concentrations. As a result, the OLEDs with 2 wt% **TPPO-tBu-DiKTa** and 5 wt% **TPA-tBu-DiKTa** in mCP:PPT cohost achieved blue and green emission at 480 and 508 nm and showed high EQE_{max} of 24.4% and 31.0%. In addition, the device with 25 wt% **TPA-tBu-DiKTa** shows broader emission yet maintained its high EQE_{max} and showed reduced efficiency roll-off. The two emitters can also enable electrochemical doping and narrowband emission in LEC devices. When included into a mobility-balanced 26DCzPPy:TCTA host matrix, the optimized **TPA-tBu-DiKTa** LEC, equipped with air-stable electrodes, delivered stable narrowband blue emission with an EQE_{max} of 2.6% at a significant luminance of 425 cd m^{-2}. The OLED and LEC with **TPA-tBu-DiKTa** each show the highest EQE_{max} among all the respective devices with **DiKTa**-based MR-TADF emitters. The outstanding performance of these devices attests to the value of the emitter design in **TPA-tBu-DiKTa** whereby the MR-TADF core is decorated with *ortho*-disposed electron-donating groups, which aid in the suppression of ACQ and enhancement of RISC.

ACKNOWLEDGMENTS

Jingxiang Wang thanks the China Scholarship Council (202006250026). We thank the Engineering and Physical Sciences Research Council (EP/R035164/1, EP/W015137/1, and EP/W007517/1) for support. Ludvig Edman and Shi Tang acknowledge financial support from the Swedish Research Council (2019-02345 and 2021–04778), the Swedish Energy Agency (50779-1 and P2021-00032), the Wallenberg Initiative Materials Science for Sustainability (WISE) funded by the Knut and Alice Wallenberg Foundation (WISE-AP01-D02), and the European Research Council for an ERC Advanced Grant (Project 101096650).

CONFLICT OF INTEREST STATEMENT

The authors declare no conflicts of interest.

DATA AVAILABILITY STATEMENT

The research data supporting this publication can be accessed at https://doi.org/10.17630/e449e75a-1ee9-4490-909c-e3913052cce1.

ORCID

Hassan Hafeez https://orcid.org/0000-0001-9647-008X
Ludvig Edman https://orcid.org/0000-0003-2495-7037
Eli Zysman-Colman https://orcid.org/0000-0001-7183-6022

REFERENCES

1. C. W. Tang, S. A. VanSlyke, *Appl. Phys. Lett.* **1987**, *51*, 913.
2. H. Uoyama, K. Goushi, K. Shizu, H. Nomura, C. Adachi, *Nature* **2012**, *492*, 234.
3. M. Y. Wong, E. Zysman-Colman, *Adv. Mater.* **2017**, *29*, 1605444.
4. M. Karaman, A. Kumar Gupta, S. Madayanad Suresh, T. Matulaitis, L. Mardegan, D. Tordera, H. J. Bolink, S. Wu, S. Warriner, I. D. Samuel, E. Zysman-Colman, *Beilstein J. Org. Chem.* **2022**, *18*, 1311.
5. S. Tang, P. Lundberg, Y. Tsuchiya, J. Ràfols-Ribé, Y. Liu, J. Wang, C. Adachi, L. Edman, *Adv. Funct. Mater.* **2022**, *32*, 2205967.
6. S. Kanagaraj, A. Puthanveedu, Y. Choe, *Adv. Funct. Mater.* **2020**, *30*, 1907126.
7. Q. Zhang, J. Li, K. Shizu, S. Huang, S. Hirata, H. Miyazaki, C. Adachi, *J. Am. Chem. Soc.* **2012**, *134*, 14706.
8. Y. Im, M. Kim, Y. J. Cho, J.-A. Seo, K. S. Yook, J. Y. Lee, *Chem. Mater.* **2017**, *29*, 1946.

9. T. Hatakeyama, K. Shiren, K. Nakajima, S. Nomura, S. Nakatsuka, K. Kinoshita, J. Ni, Y. Ono, T. Ikuta, *Adv. Mater.* **2016**, *28*, 2777.
10. D. Hall, S. M. Suresh, P. L. dos Santos, E. Duda, S. Bagnich, A. Pershin, P. Rajamalli, D. B. Cordes, A. M. Z. Slawin, D. Beljonne, A. Köhler, I. D. W. Samuel, Y. Olivier, E. Zysman-Colman, *Adv. Optical Mater.* **2020**, *8*, 1901627.
11. Y. Yuan, X. Tang, X. Y. Du, Y. Hu, Y. J. Yu, Z. Q. Jiang, L. S. Liao, S. T. Lee, *Adv. Optical Mater.* **2019**, *7*, 1801536.
12. X. Li, Y. Z. Shi, K. Wang, M. Zhang, C. J. Zheng, D. M. Sun, G. L. Dai, X. C. Fan, D. Q. Wang, W. Liu, Y. Q. Li, J. Yu, X. M. Ou, C. Adachi, X. H. Zhang, *ACS Appl. Mater. Interfaces* **2019**, *11*, 13472.
13. D. Sun, S. M. Suresh, D. Hall, M. Zhang, C. Si, D. B. Cordes, A. M. Z. Slawin, Y. Olivier, X. Zhang, E. Zysman-Colman, *Mater. Chem. Front.* **2020**, *4*, 2018.
14. X. Qiu, G. Tian, C. Lin, Y. Pan, X. Ye, B. Wang, D. Ma, D. Hu, Y. Luo, Y. Ma, *Adv. Optical Mater.* **2021**, *9*, 2001845.
15. F. Huang, K. Wang, Y. Z. Shi, X. C. Fan, X. Zhang, J. Yu, C. S. Lee, X. H. Zhang, *ACS Appl. Mater. Interfaces* **2021**, *13*, 36089.
16. S. Wu, W. Li, K. Yoshida, D. Hall, S. Madayanad Suresh, T. Sayner, J. Gong, D. Beljonne, Y. Olivier, I. D. W. Samuel, E. Zysman-Colman, *ACS Appl. Mater. Interfaces* **2022**, *14*, 22341.
17. S. Y. Yang, S. N. Zou, F. C. Kong, X. J. Liao, Y. K. Qu, Z. Q. Feng, Y. X. Zheng, Z. Q. Jiang, L. S. Liao, *Chem. Commun.* **2021**, *57*, 11041.
18. Y.-J. Yu, S.-N. Zou, C.-C. Peng, Z.-Q. Feng, Y.-K. Qu, S.-Y. Yang, Z.-Q. Jiang, L.-S. Liao, *J. Mater. Chem. C* **2022**, *10*, 4941.
19. J.-F. Liu, S.-N. Zou, X. Chen, S.-Y. Yang, Y.-J. Yu, M.-K. Fung, Z.-Q. Jiang, L.-S. Liao, *Mater. Chem. Front.* **2022**, *6*, 966.
20. S. Wu, A. Kumar Gupta, K. Yoshida, J. Gong, D. Hall, D. B. Cordes, A. M. Z. Slawin, I. D. W. Samuel, E. Zysman-Colman, *Angew. Chem. Int. Ed.* **2022**, *61*, e202213697.
21. T. Wang, A. K. Gupta, D. B. Cordes, A. M. Slawin, E. Zysman-Colman, *Adv. Optical Mater.* **2023**, *11*, 2300114.
22. J. M. dos Santos, C.-Y. Chan, S. Tang, D. Hall, T. Matulaitis, D. B. Cordes, A. M. Z. Slawin, Y. Tsuchiya, L. Edman, C. Adachi, Y. Olivier, E. Zysman-Colman, *J. Mater. Chem. C* **2023**, *11*, 8263.
23. C. Cao, J. H. Tan, Z. L. Zhu, J. D. Lin, H. J. Tan, H. Chen, Y. Yuan, M. K. Tse, W. C. Chen, C. S. Lee, *Angew. Chem. Int. Ed.* **2023**, *62*, e202215226.
24. X. C. Fan, K. Wang, Y. Z. Shi, J. X. Chen, F. Huang, H. Wang, Y. N. Hu, Y. Tsuchiya, X. M. Ou, J. Yu, C. Adachi, X. H. Zhang, *Adv. Optical Mater.* **2022**, *10*, 2101789.
25. H. Min, I. S. Park, T. Yasuda, *Angew. Chem. Int. Ed.* **2021**, *60*, 7643.
26. L. Chen, J.-H. Cai, Y.-J. Yu, Y.-K. Qu, S.-Y. Yang, S.-N. Zou, R.-H. Liu, D.-Y. Zhou, L.-S. Liao, Z.-Q. Jiang, *Sci. China Chem.* **2024**, *67*, 351.
27. S. Wu, L. Zhang, J. Wang, A. Kumar Gupta, I. D. W. Samuel, E. Zysman-Colman, *Angew. Chem. Int. Ed.* **2023**, *62*, e202305182.
28. K. Stavrou, A. Danos, T. Hama, T. Hatakeyama, A. Monkman, *ACS Appl. Mater. Interfaces* **2021**, *13*, 8643.
29. Y. Zhang, J. Wei, D. Zhang, C. Yin, G. Li, Z. Liu, X. Jia, J. Qiao, L. Duan, *Angew. Chem. Int. Ed.* **2022**, *61*, e202113206.
30. H. Liu, H. Liu, J. Fan, J. Guo, J. Zeng, F. Qiu, Z. Zhao, B. Z. Tang, *Adv. Optical Mater.* **2020**, *8*, 2001027.
31. H. Liu, J. Zeng, J. Guo, H. Nie, Z. Zhao, B. Z. Tang, *Angew. Chem. Int. Ed.* **2018**, *57*, 9290.
32. R. Aoki, R. Komatsu, K. Goushi, M. Mamada, S. Y. Ko, J. W. Wu, V. Placide, A. D'Aléo, C. Adachi, *Adv. Optical Mater.* **2021**, *9*, 2001947.
33. S. Tang, J. M. dos Santos, J. Ràfols-Ribé, J. Wang, E. Zysman-Colman, L. Edman, *Adv. Funct. Mater.* **2023**, *33*, 2306170.
34. J. Wang, T. Matulaitis, S. Pagidi, E. Zysman-Colman, *SID Symp. Dig. Tech. Pap.* **2021**, *52*, 312.
35. T. H. Dunning Jr., *J. Chem. Phys.* **1989**, *90*, 1007.
36. C. Adamo, V. Barone, *J. Chem. Phys.* **1999**, *110*, 6158.
37. A. Pershin, D. Hall, V. Lemaur, J. C. Sancho-Garcia, L. Muccioli, E. Zysman-Colman, D. Beljonne, Y. Olivier, *Nat. Commun.* **2019**, *10*, 597.
38. D. Hall, J. C. Sancho-García, A. Pershin, G. Ricci, D. Beljonne, E. Zysman-Colman, Y. Olivier, *J. Chem. Theory Comput.* **2022**, *18*, 4903.
39. N. Mataga, Y. Kaifu, M. Koizumi, *Bull. Chem. Soc. Jpn.* **1956**, *29*, 465.
40. E. Lippert, *Z. Elektrochem.* **1957**, *61*, 962.
41. J. Wang, X. Zhai, C. Ji, M. Zhang, C. Yao, G. Xie, J. Zhang, X. Xi, *Dyes Pigm.* **2023**, *219*, 111586.
42. X. Wu, B.-K. Su, D.-G. Chen, D. Liu, C.-C. Wu, Z.-X. Huang, T.-C. Lin, C.-H. Wu, M. Zhu, E. Y. Li, W.-Y. Hung, W. Zhu, P.-T. Chou, *Nat. Photonics* **2021**, *15*, 780.
43. J. Wang, Y. Yang, F. Gu, X. Zhai, C. Yao, J. Zhang, C. Jiang, X. Xi, *ACS Appl. Mater. Interfaces* **2023**, *15*, 59643.
44. J. Luo, Z. Xie, J. W. Y. Lam, L. Cheng, H. Chen, C. Qiu, H. S. Kwok, X. Zhan, Y. Liu, D. Zhu, B. Z. Tang, *Chem. Commun.* **2001**, 1740.
45. H. Chen, J. Zeng, R. Huang, J. Wang, J. He, H. Liu, D. Yang, D. Ma, Z. Zhao, B. Z. Tang, *Aggregate* **2023**, *4*, e244.
46. M. H. Tsai, Y. H. Hong, C. H. Chang, H. C. Su, C. C. Wu, A. Matoliukstyte, J. Simokaitiene, S. Grigalevicius, J. V. Grazulevicius, C. P. Hsu, *Adv. Mater.* **2007**, *19*, 862.
47. H. Miranda-Salinas, J. Wang, A. Danos, T. Matulaitis, K. Stavrou, A. P. Monkman, E. Zysman-Colman, *J. Mater. Chem. C* **2024**, *12*, 1996.
48. N. G. Connelly, W. E. Geiger, *Chem. Rev.* **1996**, *96*, 877.
49. H. Sasabe, Y. Chikayasu, S. Ohisa, H. Arai, T. Ohsawa, R. Komatsu, Y. Watanabe, D. Yokoyama, J. Kido, *Front. Chem.* **2020**, *8*, 427.
50. Q. Pei, G. Yu, C. Zhang, Y. Yang, A. J. Heeger, *Science* **1995**, *269*, 1086.
51. P. Matyba, K. Maturova, M. Kemerink, N. D. Robinson, L. Edman, *Nat. Mater.* **2009**, *8*, 672.
52. K. Yasuji, T. Sakanoue, F. Yonekawa, K. Kanemoto, *Nat. Commun.* **2023**, *14*, 992.
53. A. Sandström, H. F. Dam, F. C. Krebs, L. Edman, *Nat. Commun.* **2012**, *3*, 1002.
54. J. Zimmermann, L. Porcarelli, T. Rödlmeier, A. Sanchez-Sanchez, D. Mecerreyes, G. Hernandez-Sosa, *Adv. Funct. Mater.* **2018**, *28*, 1705795.
55. X. Dong, S. Wang, C. Gui, H. Shi, F. Cheng, B. Z. Tang, *Tetrahedron* **2018**, *74*, 497.
56. J. Ràfols-Ribé, X. Zhang, C. Larsen, P. Lundberg, E. M. Lindh, C. T. Mai, J. Mindemark, E. Gracia-Espino, L. Edman, *Adv. Mater.* **2022**, *34*, 2107849.

SUPPORTING INFORMATION

Additional supporting information can be found online in the Supporting Information section at the end of this article.

How to cite this article: J. Wang, H. Hafeez, S. Tang, T. Matulaitis, L. Edman, I. D. W. Samuel, E. Zysman-Colman, *Aggregate* **2024**, e571. https://doi.org/10.1002/agt2.571